

The structure elucidation of mequindox and 1,4-bisdesoxyequindox: NMR analyses, FT-IR spectra, DFT calculations and thermochemical studies

Jiaheng Zhang^a, Xin He^a, Haixiang Gao^{a,b,*}

^a Department of Applied Chemistry, China Agricultural University, Yuanmingyuan West Road 2#, Haidian District, Beijing 100194, PR China

^b Hubei Key Laboratory of Pollutant Analysis & Reuse Technology, Hubei Normal University, Huangshi 435002, PR China

ARTICLE INFO

Article history:

Received 6 July 2011

Accepted 22 July 2011

Available online 10 August 2011

Keywords:

Mequindox

1,4-Bisdesoxyequindox

DFT

Infrared spectra

NMR

BDE

ABSTRACT

In the current work, we report a combined experimental and theoretical study on the molecular conformation, vibrational spectra, and nuclear magnetic resonance (NMR) spectra of mequindox (MEQ) and 1,4-bisdesoxyequindox (1,4-BDM). The geometric structure and vibrational frequencies of MEQ and 1,4-BDM have been calculated by density functional theory employing the B3LYP functional and 6-311++G(d,p) basis set. The ¹H and ¹³C NMR chemical shifts have been calculated by gauge-including atomic orbital method with B3LYP 6-311++G(2df,2pd) approach. The calculation results have been applied to simulate the infrared and NMR spectra of the compounds. The theoretical results agree well with the observed spectra. The bond dissociation enthalpy of MEQ and the heat of formation of MEQ and 1,4-BDM have also been computed.

© 2011 Elsevier B.V. All rights reserved.

1. Introduction

Quinoxaline 1,4-dioxide derivatives (QdNOs) are an important class of benzoheterocycles that consist of one or two acyclic chain moieties combined with a quinoxaline ring. Some QdNOs have been regarded as interesting biologically active compounds and have been utilized in the pharmaceutical, veterinary, and industrial chemical fields since the 1970s [1]. With the development of the domestic animal drug industry in the last decade, these compounds have been widely used on cattle, swine, fish, and poultry at subtherapeutic levels for improving feed efficiency [2]. These drugs ameliorate the intestinal microflora, improve protein utilization, and increase protein synthesis *in vivo* [3].

Mequindox (2-methyl-3-acetylquinoxaline-1,4-dioxide; C₁₁H₁₀N₂O₃; MEQ) is a novel synthetic QdNO derivative used as an antibacterial by the Lanzhou Institute of Animal Husbandry and Veterinary Drugs, Chinese Academy of Agriculture Sciences to treat pig treponeme dysentery. Although this novel compound has presented good antibiotic activity and growth-enhancing activity, the cytotoxicity, genotoxicity, and metabolomics of MEQ have not been studied thoroughly [4].

In our previous studies, the toxicity of MEQ was determined to be closely associated with the deoxidized metabolites, and the isomeric

1- and 4-mono-N-oxides of MEQ were synthesized [5,6]. However, only a few articles on 1,4-bisdesoxyequindox (1,4-BDM) have been published, as the di-reduction products of the N-oxide moiety of MEQ. Hence, obtaining detailed structure-related parameters and vibrational frequencies, as well as nuclear magnetic resonance (NMR) studies of these desoxy metabolites and their parent compound are important.

NMR is arguably one of the most sensitive and versatile analytical probes of molecular structure and dynamics of complex organic compounds. Recently, there has been increasing interest in the use of density functional theory (DFT) to aid NMR analysis [7]. The studies of Chesnut [8] and Sauer et al. [9] in 1997 demonstrated that the ¹H chemical shifts of small molecules can be obtained at accuracies of ca. ±0.1 ppm. When some larger basis sets are employed, the accuracy of the calculation is still acceptable in the case of complex targets.

In the research of Rablen et al., the GIAO/B3LYP/6-311++G** model was found to be a promising alternative. It showed the best cost-to-performance ratio and provided predictions with a root-mean-square deviation of <0.2 ppm for 80 medium-sized molecules [10].

Although much effort has gone into aiding these methods by developing procedures and adjusting vibrational frequency scale factors, only a few analyses of QdNO vibrational spectra have been done using DFT methods. Yurdakul and Polat studied the Fourier transform infrared (FT-IR) spectra of 2-hydroxyquinoxaline using the B3LYP/6-311++G** DFT method, and they observed that the infrared absorption of QdNOs computed by this method agree

* Corresponding author at: Department of Applied Chemistry, China Agricultural University, Yuanmingyuan West Road 2#, Haidian District, Beijing 100194, PR China. Tel.: +86 10 62734876; fax: +86 10 62733830.

E-mail address: hxgao@cau.edu.cn (H. Gao).

reasonably well with the experimental data [11]. In the study of Miranda et al., a new heterocyclic dipyrrodo[3,2-f:2',3'-h]quinoxalino[2,3-b]quinoxaline was synthesized and characterized by IR spectroscopy, ^1H NMR and ^{13}C NMR spectroscopy, and DFT calculation [12].

With the development of investigations on the toxicity mechanism of QdNOs, several studies involving experimental validation or theoretical calculation have resulted in remarkable achievements [13–15]. Recently, attention has been paid to the detailed thermodynamic analysis of the homolytic N–O cleavage and the formation of HO \cdot radicals, which leads to cytotoxicity by cleaving DNA strands. Thus, the N–O bond strength, which can be measured by the N–O bond dissociation enthalpies (BDEs), should be investigated [16–18]. Therefore, the calculation of N–O BDEs has been a strategic goal in understanding the toxic properties of QdNOs.

In the current study, 1,4-BDM was synthesized from MEQ, and DFT calculations were done to obtain the theoretical ^1H NMR, ^{13}C NMR chemical shifts and vibrational frequencies. We also report the experimental NMR and IR spectra of these QdNOs to compare their calculated values and detect any relation between the values. Moreover, heat of formation (HOF) of MEQ and 1,4-BDM was calculated.

2. Experimental

2.1. Synthesis

A solution of mequindox (12 g, 0.055 mol) in 95% EtOH (240 ml) was heated under reflux for 0.5 h then sodium hydrosulphite (18 g, 0.104 mol) was added in portions. The mixture was heated under reflux for 2 h, dilute with cold water and the reaction mixture was extracted with chloroform (3 \times 50 ml). The combined chloro-

form extracts were dried over anhydrous magnesium sulfate, filtered and evaporated to dryness under vacuum. The residue was purified by recrystallized from ether to yield a pale yellow acicular crystal product of 1,4-bisdesoxyquinoxalox (8.3 g, 0.0045 mol). Yield: 82%; m.p. 85.2–86.1 $^\circ\text{C}$; MS(ESI) m/z (%): 187.10 $[\text{M}+\text{H}]^+$. HRMS(ESI) calcd for $\text{C}_{11}\text{H}_{11}\text{N}_2\text{O}$ $[\text{M}+\text{H}]^+$ 187.2213, found 187.0954.

2.2. Methods and calculations

Mequindox (98%) was provided by College of Veterinary Medicine, Huazhong Agricultural University (Wuhan, China). Sodium hydrosulphite was purchased from Sigma–Aldrich. Other chemicals used in synthesis were purchased from Guoyao chemical Co. (Shanghai, China).

^1H and ^{13}C NMR spectra for solutions (in CDCl_3 using tetramethylsilane as internal standard) were recorded on a BrukerDSX-300 instrument. Mequindox forms yellow powder whereas 1,4-bisdesoxyquinoxalox forms pale yellow crystal at room temperature. IR spectra of both the molecules were recorded in KBr disc. Perkin-Elmer FT-IR Spectrum 100 spectrometer was used to record the IR spectra in the spectral range 450–4000 cm^{-1} . The spectrum was recorded with a scanning speed of 10 $\text{cm}^{-1} \text{min}^{-1}$ and the spectral resolution of 4.0 cm^{-1} .

Full geometry optimizations of isolated molecules were accomplished by means of hybrid functional B3LYP [19,20] and the 6-311++G(d,p) basis set with the Gaussian 09 code [21]. The optimized structural parameters were used in the vibrational frequency calculations at DFT B3LYP 6-311++G(d,p) level. The calculated vibrational wave numbers were scaled with the scale factor, yielding a good agreement between calculated assignments and experimental data. The calculation of potential energy distribution (PED) was done by GAR2PED software package [22] and assisted by

Table 1
Calculated geometry structure of MAQM.

Bond length (Å)	MEQ	1,4-BDM	Exp.	Bond angle ($^\circ$)	MEQ	1,4-BDM	Exp.
C1–C2	1.378	1.373	1.377	C1–C2–C3	119.18	119.68	119.9
C2–C3	1.405	1.418	1.401	C2–C3–C4	120.28	119.83	119.0
C3–C4	1.407	1.424	1.401	C3–C4–C5	119.91	119.26	120.9
C4–C5	1.405	1.416	1.404	C4–C5–C6	119.29	119.79	120.6
C5–C6	1.378	1.375	1.359	C5–C6–C1	120.74	120.92	121.5
C1–C6	1.410	1.418		C6–C1–C2	120.60	120.52	120.0
C13–C14	1.404	1.447	1.406	C13–C14–C17	121.92	123.04	
C14–C17	1.524	1.513	1.514	C14–C17–C19	117.19	117.24	
C13–C23	1.492	1.503	1.477	C14–C13–C23	124.53	123.80	
C17–C19	1.506	1.513		H7–C1–C2	119.64	120.08	120.1
C3–N12	1.399	1.354	1.380	H8–C2–C1	122.86	122.03	120.1
C4–N11	1.401	1.359	1.388	H9–C5–C4	117.90	118.20	120.1
C13–N11	1.359	1.318	1.357	H10–C6–C1	119.70	119.25	119.3
C14–N12	1.352	1.318	1.309	C3–C4–N11	120.26	120.78	
N11–O16	1.279		1.296	C4–C3–N12	119.75	120.00	121.6
N12–O15	1.283			C3–N12–C14	118.49	118.59	116.8
C17–O18	1.208	1.216		C4–N11–C13	119.09	119.03	120.1
C1–H7	1.083	1.084	0.950	N12–C14–C13	122.38	121.77	125.2
C2–H8	1.081	1.084	0.950	N11–C13–C14	120.02	119.81	117.5
C5–H9	1.081	1.083	0.950	C4–N11–O16	119.84		120
C6–H10	1.084	1.084	0.950	C3–N12–O15	120.10		
C19–H20	1.097	1.089		C13–C14–C17	121.92	123.04	119.0
C19–H21	1.090	1.092		C14–C13–C23	124.53	123.80	127.3
C19–H22	1.090	1.092		C14–C17–O18	119.01	121.22	
C23–H24	1.094	1.092	0.980	C14–C17–C19	117.19	117.24	
C23–H25	1.086	1.092	0.980	C17–C19–H20	108.26	108.45	
C23–H26	1.093	1.092	0.980	C17–C19–H21	111.05	110.65	
Selected dihedral angles				C17–C19–H22	109.44	110.65	
C5–C4–N11–C13	–179.54	–180.00	–179.5	C13–C23–H24	109.58	111.37	109.5
C2–C3–N12–C14	179.70	180.00	179.4	C13–C23–H25	111.80	111.37	109.5
C4–N11–C13–C23	179.85	179.99	178.7	C13–C23–H26	109.58	108.27	109.5
C3–N12–C14–C17	179.33	179.99	176.9				
C13–C14–C17–O18	–61.07	–0.01					
C13–C14–C17–C19	114.91	179.99					

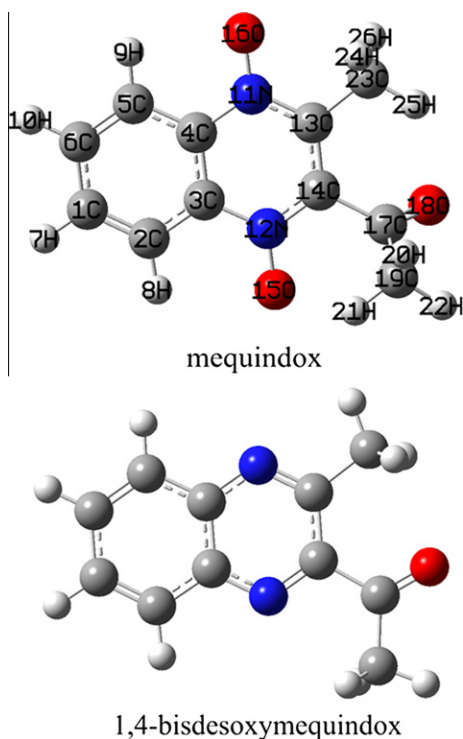


Fig. 1. Optimized molecular structures and atomic numbering of meq and 1,4-BDM.

MOLEKEL program which offers visualized presentation of vibration modes [23,24]. Nuclear shielding were computed at IEFPCM/B3LYP 6-311++G(2df,2pd) basis set by the gauge-including atomic orbital (GIAO) method. The SCRF theory via integral equation formalism version of the polarizable continuum model (IEFPCM) including the effect of environment was applied to correct the relative ground state energies obtained for isolated molecules in gas phase. The ^1H and ^{13}C chemical shifts is obtained as $\delta = \sigma_{\text{ref}} - \sigma$, where σ_{ref} is the shielding constant of ^1H and ^{13}C in tetramethylsilane (TMS) and σ is the corresponding reference parameter in the molecule of interest. Subsequently, the B3LYP 6-311++G(2df,2pd) approach was used to further optimize the geometry and to obtain the natural population analysis of these two compounds. The absolute enthalpies of all compounds were used to estimate the standard molar enthalpies of formation and enthalpies of N–O bond dissociation are B3LYP 6-311++G(2df,2pd) values.

3. Results and discussion

3.1. Geometrical structure

The optimized structural parameters of MEQ and 1,4-BDM calculated by the DFT-B3LYP level with 6-311++G(d,p) as the basis sets are listed in Table 1, in accordance with the atom numbering scheme of the molecule shown in Fig. 1. Since the exact crystal structures of these compounds are not available at present, the optimized structures can only be compared with 3-methylquinoxaline-2-carboxylic acid 4-oxide, which has a highly similar crystal structure (determined by X-ray studies) [25]. As shown in Table 1, most of the computed bond lengths and bond angles are slightly larger than the corresponding experimental data. This can be explained by the fact that the experimental results were based on the solid phase, whereas theoretical calculations were based on the gaseous phase, wherein intermolecular Coulombic interactions among neighboring molecules were ignored.

The DFT data show that the C–C bond length is 1.373–1.524 Å. In the case of C–H bonds, C19–H20 of MEQ is the longest, whereas

the C2–H8 and C5–H9 bonds are the shortest, and the rest fall in the range of 1.081–1.097 Å. In addition, N11–O16 and N12–O15 in MEQ, and C17–O18 in MEQ and 1,4-BDM have lengths of 1.279, 1.283, 1.208, and 1.206 Å, respectively.

In MEQ and 1,4-BDM, the calculated values of the C–C angles for the benzene ring are around the typical hexagonal angle of 120° , in contrast to the quinoxaline ring, in which the substitution leads to some changes in the bond angles.

C3–N12–C14 and N12–C14–C13 in MEQ and 1,4-BDM show an obvious deviation from 120° and are consistent with the experimental values. The benzene ring and quinoxaline moiety are essentially planar, as evident in the dihedral angles of C5–C4–N11–C13 (-179.54 for MEQ and -180.00 for 1,4-BDM) and C2–C3–N12–C14 (179.70 for MEQ and 180.00 for 1,4-BDM). This finding agrees with the characteristics of other substituted quinoxalines [26].

3.2. Vibrational frequency

Theoretical (unscaled and scaled) and experimental vibrational frequencies (cm^{-1}), peak intensities (km mol^{-1}) and the assignments of IR spectra of MEQ and 1,4-BDM.

MEQ consists of 26 atoms, so it has 72 normal vibrational modes; it belongs to the point group C_1 . 1,4-BDM, which has 24 atoms and 66 normal modes of fundamental vibrations resulting from the di-reduction of the N-oxide moiety of MEQ, also possesses C_1 point group symmetry. The frequencies calculated at B3LYP levels are overestimated compared with the experimental values. This is due to neglect of the anharmonicity present in real systems. Regardless of the level of calculations, the calculated harmonic frequencies are usually scaled down to improve agreement with the experimental values; in the current study, the scaling factor 0.9668 was used [27].

Assignments of several vibrational frequencies in the experimental FT-IR spectra of MEQ and 1,4-BDM are shown in Table 2. The theoretical wavenumbers (unscaled and scaled) for the various fundamental vibrational modes predicted by DFT methods using the 6-311++G(d,p) basis set are presented in Table 2. IR spectra from experiments and those predicted by the DFT B3LYP method are shown in Figs. 2 and 3.

For all aromatic compounds, the carbon–hydrogen stretching vibrations commonly appear in the region of $3000\text{--}3100\text{ cm}^{-1}$ [28]. In the experimental spectrum, the C–H stretching frequencies are slightly over 3100 cm^{-1} (3104 cm^{-1} for MEQ and 3103 cm^{-1} for 1,4-BDM). Scaled theoretical C–H stretching modes were found to be $3058, 3072, 3101, \text{ and } 3102\text{ cm}^{-1}$ for MEQ, and $3065, 3076, 3088, \text{ and } 3093\text{ cm}^{-1}$ for 1,4-BDM. The vibrations assigned to aromatic C–H stretch predicted theoretically at B3LYP/6-311++G(d,p) are in good agreement with the experimental assignment. As indicated by the TED, these modes involve approximately 100% contribution suggesting that they are pure stretching modes. CH_3 stretching modes were found in the region $2922\text{--}3064\text{ cm}^{-1}$ for MEQ and $2947\text{--}3042\text{ cm}^{-1}$ for 1,4-BDM. The C–H in-plane bending frequencies are within $1000\text{--}1300\text{ cm}^{-1}$ and the three out-of-plane bending vibrations are in the range of $750\text{--}1000\text{ cm}^{-1}$.

The C–H in-plane bending vibrations of MEQ and 1,4-BDM are all within $1097\text{--}1328\text{ cm}^{-1}$; these correlate well with the frequencies calculated by the DFT method ($1083\text{--}1321\text{ cm}^{-1}$ for MEQ and $1109\text{--}1323\text{ cm}^{-1}$ for 1,4-BDM). The C–H out-of-plane vibration was observed at 776 cm^{-1} for both molecules, with theoretical wavenumbers of 761 cm^{-1} for MEQ and 753 cm^{-1} for 1,4-BDM. Two peaks at 1446 cm^{-1} for MEQ and 1416 cm^{-1} for 1,4-BDM were also observed, and were assigned to the scissoring of CH_3 , which has predicted frequencies at 1439 cm^{-1} and 1426 cm^{-1} .

The strong experimental IR band observed at 1515 cm^{-1} in MEQ was assigned to C–C stretching; a similar peak in the 1,4-BDM spectrum (at 1514 cm^{-1}) has medium intensity.

Table 2
Theoretical (unscaled and scaled) and experimental vibrational frequencies (cm^{-1}), peak intensities (km mol^{-1}) and the assignments of IR spectra of MEQ and 1,4-BDM.

Mode	MEQ			Exp.	Assignment	1,4-BDM			Exp.	Assignment
	Unscaled freq.	Scaled freq.	Intensity			Unscaled freq.	Scaled freq.	Intensity		
1	55	53	3.2		$\tau\text{NCCO}(100)$	26	25	4.1		$\tau\text{NCCC}(59)$, $\tau\text{NCCO}(32)$
2	68	66	2.9		$\tau\text{NCCO}(100)$	71	69	0.0		$\beta\text{C}-\text{C}(59)$, $\beta\text{Ring}(19)$
3	91	88	3.1		$\tau\text{OCCH}(100)$	116	112	2.4		$\gamma\text{Ring}(48)$, $\gamma\text{CH}_3(38)$
4	101	98	6.2		$\tau\text{OCCH}(100)$	123	119	0.0		$\tau\text{CCCH}(98)$
5	136	131	0.6		$\tau\text{NCCH}(64)$, $\tau\text{NCCO}(35)$	175	169	2.7		$\delta\text{NCC}(80)$
6	162	157	2.0		$\tau\text{NCCH}(51)$, $\beta\text{N}-\text{O}(25)$	200	193	0.5		$\tau\text{CCCH}(95)$
7	163	158	0.1		$\tau\text{NCCH}(50)$, $\beta\text{N}-\text{O}(26)$	242	234	1.4		$\gamma\text{Ring}(83)$
8	193	187	3.8		$\gamma\text{N}-\text{O}(57)$, $\tau\text{NCCH}(20)$	296	286	0.0		$\gamma\text{Ring}(79)$
9	234	226	3.2		$\gamma\text{Ring}(82)$, $\beta\text{CH}_3(17)$	307	297	4.1		$\gamma\text{CH}_3(76)$
10	277	268	2.0		$\beta\text{CH}_3(51)$, $\gamma\text{Ring}(31)$	335	324	2.2		$\delta\text{CCC}(72)$, $\delta\text{CNC}(13)$
11	306	296	4.1		$\gamma\text{Ring}(56)$, $\beta\text{N}-\text{O}(20)$, $\beta\text{C}-\text{C}(17)$	379	366	4.1		$\delta\text{CCC}(50)$, $\delta\text{CNC}(40)$
12	352	340	0.6		$\beta\text{CH}_3(68)$, $\beta\text{N}-\text{O}(25)$	430	416	8.5		$\beta\text{Ring}(59)$, $\beta\text{CH}_3(32)$
13	362	350	0.1		$\gamma\text{CH}_3(93)$	472	456	0.2		$\delta\text{NCC}(58)$, $\delta\text{CCC}(21)$
14	404	391	22.7		$\beta\text{N}-\text{O}(86)$	500	483	0.0		$\gamma\text{Ring}(55)$, $\gamma\text{C}-\text{H}(41)$
15	423	409	0.5		$\gamma\text{Ring}(84)$, $\beta\text{N}-\text{O}(14)$	511	494	0.1		$\gamma\text{Ring}(96)$
16	452	437	2.0		$\delta\text{NCC}(97)$	524	507	8.2		$\delta\text{NCC}(71)$, $\beta\text{C}=\text{O}(25)$
17	459	444	3.0	457vw	$\gamma\text{Ring}(92)$	593	573	0.0	552vw	$\gamma\text{Ring}(91)$
18	503	486	5.0		$\gamma\text{Ring}(63)$, $\gamma\text{CH}_3(14)$	597	577	14.6	573vw	$\delta\text{CCC}(66)$, $\beta\text{C}=\text{O}(21)$
19	515	498	2.0	515w	$\delta\text{CNC}(39)$, $\gamma\text{C}=\text{O}(30)$, $\delta\text{CCC}(24)$	630	609	1.3	615 m	$\delta\text{CCC}(47)$, $\delta\text{CNC}(23)$
20	561	542	4.6	552w	$\delta\text{CCC}(63)$, $\gamma\text{C}=\text{O}(33)$	657	635	26.3	637w	$\delta\text{CCC}(68)$, $\beta\text{C}-\text{C}(17)$
21	568	549	4.2	573w	$\gamma\text{Ring}(52)$, $\gamma\text{C}=\text{O}(45)$	704	681	0.8	657w	$\beta\text{Ring}(67)$, $\beta\text{CH}_3(10)$
22	615	595	52.4	615s	$\delta\text{CCC}(40)$, $\delta\text{CCN}(2)$, $\nu\text{C}-\text{C}(27)$	721	697	1.7	683vw	$\delta\text{CNC}(57)$, $\nu\text{C}-\text{C}(17)$
23	636	615	9.7		$\beta\text{N}-\text{O}(79)$, $\beta\text{C}-\text{H}(17)$	779	753	80.3	776 m	$\gamma\text{C}-\text{H}(92)$
24	668	646	5.9	636 m	$\delta\text{CCC}(75)$, $\delta\text{CNC}(10)$	805	778	0.0		$\gamma\text{Ring}(44)$, $\gamma\text{C}-\text{H}(40)$
25	683	660	6.1	656w	$\gamma\text{C}-\text{C}(69)$, $\gamma\text{CH}_3(24)$	828	801	13.0	829 m	$\nu\text{C}-\text{C}(61)$, $\nu\text{C}-\text{N}(12)$
26	711	687	0.4	683w	$\delta\text{CCC}(89)$	882	853	0.1		$\gamma\text{C}-\text{H}(94)$
27	714	690	1.7	694w	$\delta\text{CCC}(66)$, $\gamma\text{CH}_3(24)$	917	887	1.7		$\delta\text{CCC}(39)$, $\delta\text{CNC}(28)$
28	787	761	63.9	776s	$\gamma\text{C}-\text{H}(90)$	944	913	59.8		$\nu\text{C}-\text{C}(63)$, $\beta\text{C}=\text{O}(25)$
29	845	817	13.9	830s	$\delta\text{CCC}(49)$, $\gamma\text{CH}_3(36)$	981	948	1.2		$\gamma\text{C}-\text{H}89$
30	871	842	0.6		$\delta\text{CCC}(54)$, $\nu\text{C}-\text{N}(18)$, $\nu\text{C}-\text{C}(13)$	1003	970	1.0	965w	$\gamma\text{C}-\text{H}(96)$
31	886	857	0.0	861w	$\gamma\text{C}-\text{H}(100)$	1027	993	8.8		$\gamma\text{C}-\text{H}(61)$, $\gamma\text{CH}_3(22)$
32	970	938	22.2		$\nu\text{C}-\text{C}(56)$, $\delta\text{CH}_3(28)$	1034	1000	1.3		$\gamma\text{CH}_3(74)$, $\beta\text{C}=\text{O}(12)$
33	996	963	2.7		$\gamma\text{C}-\text{H}(100)$	1036	1002	1.4		$\gamma\text{CH}_3(42)$, $\gamma\text{C}-\text{H}(34)$
34	1010	976	0.0		$\gamma\text{C}-\text{H}(100)$	1053	1018	2.1	1000w	$\gamma\text{CH}_3(78)$
35	1019	985	22.9	966 m	$\delta\text{CCC}(48)$, $\nu\text{C}-\text{C}(44)$	1076	1040	20.2	1050 m	$\gamma\text{CH}_3(73)$, $\nu\text{C}-\text{C}(20)$
36	1034	1000	3.8		$\beta\text{C}-\text{H}(49)$, $\gamma\text{CH}_3(36)$	1147	1109	22.3	1097s	$\beta\text{C}-\text{H}(91)$
37	1043	1008	11.1	1000 m	$\beta\text{C}-\text{H}(94)$	1162	1123	8.3		$\beta\text{C}-\text{H}(76)$, $\nu\text{C}-\text{N}(11)$
38	1052	1017	1.5	1016 m	$\delta\text{CH}_3(98)$	1217	1177	61.0	1149 m	$\beta\text{C}-\text{H}(42)$, $\nu\text{C}-\text{C}(29)$, $\nu\text{C}-\text{N}(16)$
39	1074	1038	55.4	1050s	$\gamma\text{CH}_3(40)$, $\nu\text{C}-\text{C}(26)$, $\gamma\text{C}=\text{O}(11)$	1259	1217	13.3	1216 m	$\nu\text{Ring}(71)$, $\beta\text{C}-\text{H}(17)$
40	1120	1083	61.1	1097s	$\beta\text{C}-\text{H}(66)$, $\nu\text{C}-\text{N}(29)$	1286	1243	26.5		$\nu\text{Ring}(62)$, $\beta\text{C}-\text{H}(17)$
41	1140	1102	1.3		$\beta\text{C}-\text{H}(46)$, $\nu\text{Ring}(41)$	1332	1288	34.9	1274 m	$\nu\text{Ring}(77)$
42	1167	1128	4.3		$\beta\text{C}-\text{H}(55)$, $\nu\text{N}-\text{O}(29)$, $\nu\text{C}-\text{N}(12)$	1345	1300	4.0		$\nu\text{C}-\text{N}(59)$, $\nu\text{C}-\text{C}(35)$
43	1215	1175	1.8	1149 m	$\beta\text{C}-\text{H}(69)$, $\nu\text{N}-\text{O}(20)$	1368	1323	1.2		$\nu\text{C}-\text{C}(39)$, $\delta\text{CH}_3(29)$, $\beta\text{C}-\text{H}(19)$
44	1225	1184	34.8	1186 m	$\beta\text{C}-\text{H}(67)$, $\nu\text{C}-\text{C}(22)$	1390	1344	42.3	1328vs	$\delta\text{CH}_3(96)$
45	1237	1196	14.7	1216 m	$\nu\text{Ring}(41)$, $\nu\text{N}-\text{O}(32)$, $\nu\text{C}-\text{C}(22)$	1411	1364	25.4		$\delta\text{CH}_3(72)$, $\nu\text{C}-\text{C}(12)$
46	1298	1255	54.2		$\nu\text{C}-\text{C}(30)$, $\nu\text{C}-\text{N}(28)$, $\beta\text{C}-\text{H}(20)$	1423	1376	22.0	1384vs	$\nu\text{Ring}(49)$, $\beta\text{C}-\text{H}(32)$
47	1362	1317	311.7	1275s	$\nu\text{N}-\text{O}(61)$, $\beta\text{C}-\text{H}(22)$	1459	1411	13.6		$\delta\text{CH}_3(88)$
48	1366	1321	126.6	1328vs	$\nu\text{N}-\text{O}(61)$, $\nu\text{Ring}(28)$	1462	1413	23.9		$\delta\text{CH}_3(58)$, $\beta\text{C}-\text{H}(19)$
49	1384	1338	29.0		$\delta\text{CH}_3(90)$	1464	1415	10.9		$\delta\text{CH}_3(99)$
50	1402	1355	4.7		$\nu\text{C}-\text{C}(91)$	1475	1426	9.3	1416 m	$\delta\text{CH}_3(87)$
51	1425	1378	0.2		$\delta\text{CH}_3(81)$	1498	1448	1.1		$\nu\text{C}-\text{C}(92)$
52	1448	1400	73.2	1383 m	$\delta\text{CH}_3(85)$, $\nu\text{C}-\text{C}(11)$	1516	1466	10.0		$\nu\text{C}-\text{C}(60)$, $\beta\text{C}-\text{H}(20)$
53	1453	1405	16.0		$\delta\text{CH}_3(85)$, $\beta\text{C}-\text{H}(11)$	1592	1539	2.3	1514 m	$\nu\text{Ring}(91)$
54	1462	1413	10.8		$\delta\text{CH}_3(81)$, $\beta\text{C}-\text{H}(12)$	1592	1539	69.1		$\nu\text{Ring}(99)$
55	1468	1419	7.3	1417s	$\nu\text{Ring}(54)$, $\beta\text{C}-\text{H}(39)$	1651	1596	3.5	1602w	$\nu\text{Ring}(287)$
56	1484	1435	10.0		$\delta\text{CH}_3(78)$	1755	1697	244.4	1700vs	$\nu\text{C}=\text{O}(96)$
57	1488	1439	2.9	1446 m	$\delta\text{CH}_3(77)$, $\beta\text{C}-\text{H}(16)$	3048	2947	1.1		$\nu\text{CH}_3(100)$
58	1534	1483	49.6	1515s	$\nu\text{Ring}(87)$	3048	2947	7.2		$\nu\text{CH}_3(100)$
59	1545	1494	3.4		$\nu\text{Ring}(74)$, $\delta\text{CH}_3(13)$	3103	3000	5.6		$\nu\text{CH}_3(99)$
60	1638	1584	3.4		$\nu\text{Ring}(83)$	3107	3004	5.0		$\nu\text{CH}_3(99)$
61	1644	1589	4.3	1602 m	$\nu\text{C}-\text{C}(88)$	3136	3032	12.8		$\nu\text{CH}_3(100)$
62	1782	1723	209.6	1701vs	$\nu\text{C}=\text{O}(99)$	3146	3042	15.0		$\nu\text{CH}_3(100)$
63	3022	2922	2.7		$\nu\text{CH}_3(99)$	3170	3065	1.8		$\nu\text{CH}(\text{Ring})(99)$
64	3044	2943	2.8		$\nu\text{CH}_3(100)$	3182	3076	4.7		$\nu\text{CH}(\text{Ring})(100)$
65	3088	2985	3.3	2970w	$\nu\text{CH}_3(100)$	3194	3088	8.6		$\nu\text{CH}(\text{Ring})(100)$
66	3105	3002	3.3		$\nu\text{CH}_3(99)$	3199	3093	11.9	3104w	$\nu\text{CH}(\text{Ring})(100)$
67	3149	3044	3.0		$\nu\text{CH}_3(100)$					
68	3169	3064	4.2		$\nu\text{CH}_3(100)$					
69	3181	3075	5.6		$\nu\text{C}-\text{H}(\text{Ring})(99)$					
70	3195	3089	7.5		$\nu\text{C}-\text{H}(\text{Ring})(100)$					

Table 2 (continued)

Mode	MEQ			Exp.	Assignment	1,4-BDM			Exp.	Assignment
	Unscaled freq.	Scaled freq.	Intensity			Unscaled freq.	Scaled freq.	Intensity		
71	3226	3119	7.6		$\nu_{\text{asC-H(Ring)}}(100)$					
72	3227	3120	3.4		$\nu_{\text{sC-H(Ring)}}(100)$					

Scaled factors: B3LYP/6-311++G(d,p): 0.9668.

ν – stretching (*s* – symmetric; *as* – asymmetric), β – in-plane, γ – out-of-plane bending, ω – wagging, δ – scissoring, τ – torsion. *s* – strong, *m* – medium, *w* – weak, *v* – very.

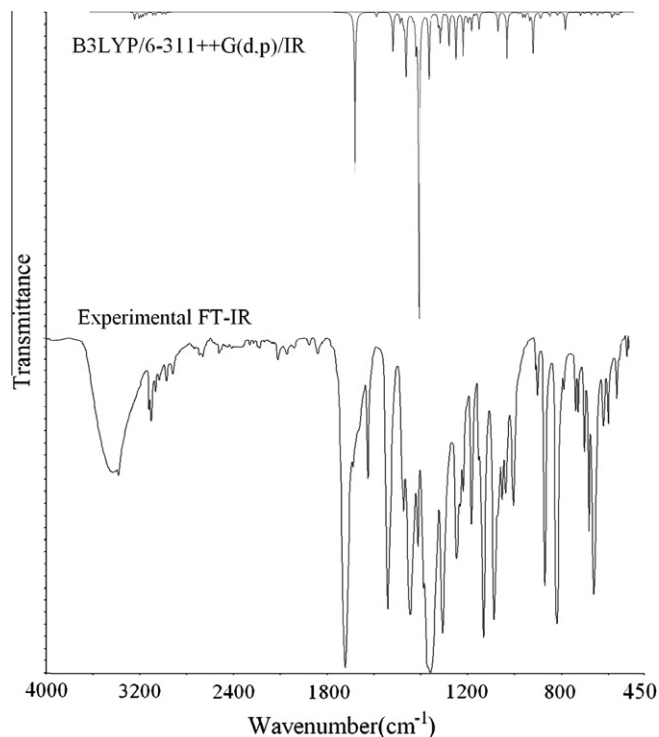


Fig. 2. Experimental and calculated FT-IR spectrums of MEQ.

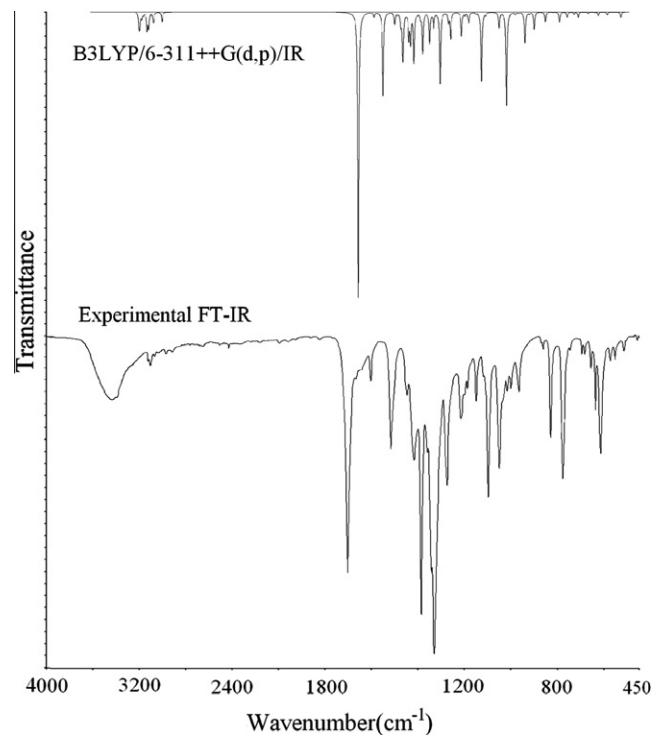


Fig. 3. Experimental and calculated FT-IR spectrums of 1,4-BDM.

Since the mixing of several bands is possible in the region, the assignment of C–N vibration is a challenging task. Moreover, most of the C–C and C–N vibrations are associated with the whole ring: vibrations occurring in the region 1417–1602 cm^{-1} and 1000–1186 cm^{-1} are assigned to $\nu_{\text{C-C}}$ (ring) and $\beta_{\text{C-H}}$ (ring). These specific bands have been also found in the IR spectrum of other quinoxaline molecules [29].

Mode No. 35 of MEQ and Mode No. 30 of 1,4-BDM at the calculated frequencies of 985 and 970 cm^{-1} , respectively, are assigned to the C–C and C–N stretching and C–N bending vibrations; corresponding bands at $\sim 965 \text{ cm}^{-1}$ were observed in the experimental FT-IR spectra. The strong bands of MEQ and 1,4-BDM observed at $\sim 615 \text{ cm}^{-1}$ are assigned to C–C and C–N bending and C–N stretching; similar bands are present in the predicted spectra, at calculated frequencies of 595 and 609 cm^{-1} .

As seen in Figs. 2 and 3, the characteristic wavenumber of the $\nu(\text{C=O})$ mode has one of the strongest bands, and the intensities for this mode (1701 cm^{-1} for MEQ and 1700 cm^{-1} for 1,4-BDM) are in accordance with the calculated values (1723 and 1697 cm^{-1}).

3.3. NMR spectra

After initial optimization of the molecular structures with the 6-311++G(d,p) basis set, gauge-including atomic orbital ^{13}C and ^1H chemical shift calculations of MEQ and 1,4-BDM were done

using the B3LYP 6-311++G(2df,2pd) basis set. In the current study, the calculated ^1H and ^{13}C isotropic chemical shielding for trimethylsilane σ_{ref} at the B3LYP/6-311++g(2df,2pd) are 31.62 and 183.67 ppm, respectively. The theoretical and experimental chemical shifts, isotropic shielding tensors, and the peak assignments for MEQ and 1,4-BDM are presented in Table 3.

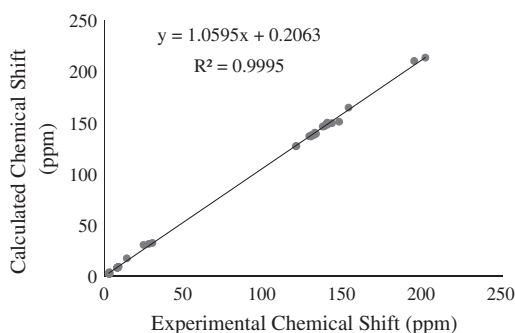
The linear correlation between the calculated and experimental values was determined, the result of which are presented in Fig. 4. A good correlation between predicted and observed ^{13}C and ^1H chemical shifts was found. To remove systematic errors and decrease deviation, the calculated values were corrected according to the equation, $\delta = \frac{\delta_{\text{calc}} - \text{intercept}}{\text{slope}}$ [30]. The slope and intercept were obtained by plotting the calculated data against the experimental shifts to be assigned. In the present study, the intercept and slope are 0.2063 and 1.0595, respectively. As demonstrated in Table 3, the mean absolute error between the calculated chemical shifts and the experimental values is 4.19 ppm, whereas the corrected mean absolute error is 0.91 ppm.

Typically, aromatic carbons give signals in overlapped areas of the spectrum, with chemical shift values from 100 to 150 ppm. The highest chemical shift of carbon is that of C17 for both MEQ and 1,4-BDM because it is linked to an electron-withdrawing ketone oxygen atom. Due to the influence of electronegative nitrogen atoms, the chemical shifts of C3, C4, C13, and C14 are significantly different in the range of 136–153 ppm. Shifts of other carbons

Table 3The experimental, calculated and corrected ^1H and ^{13}C isotropic chemical shifts (ppm) with respect to TMS of MEQ and 1,4-BDM.

Assignment	MEQ			1,4-BDM			Assignment	MEQ			1,4-BDM		
	Exp.	Cal.	Corrected	Exp.	Cal.	Corrected		Exp.	Cal.	Corrected	Exp.	Cal.	Corrected
H7	7.89	8.16	7.51	7.82	8.14	7.49	C1	131.49	137.90	129.96	128.35	136.58	128.72
H8	8.58	8.94	8.24	8.06	8.53	7.85	C2	120.23	127.06	119.73	129.75	137.70	129.77
H9	8.62	8.99	8.29	8.06	8.41	7.74	C3	136.79	145.95	137.56	139.69	147.77	139.27
H10	7.89	8.21	7.55	7.84	8.24	7.58	C4	137.86	146.31	137.90	147.08	150.71	142.05
H20	2.74	2.31	1.99	2.98	3.45	3.06	C5	120.00	126.79	119.47	129.46	136.25	128.40
H21	2.74	3.60	3.21	2.98	3.45	3.06	C6	132.54	138.95	130.95	131.87	140.08	132.02
H22	2.74	2.51	2.18	2.98	2.12	1.80	C13	139.69	149.83	141.22	153.00	164.47	155.03
H24	2.53	2.57	2.23	2.85	3.29	2.91	C14	138.89	148.33	139.81	142.57	149.28	140.70
H25	2.53	2.19	1.87	2.85	3.29	2.91	C17	194.21	210.01	198.02	201.20	213.30	201.12
H26	2.53	2.60	2.26	2.85	2.82	2.47	C19	29.90	32.32	30.31	27.69	31.46	29.50
							C23	13.84	17.34	16.17	24.34	30.41	28.51
MAE	4.19												
CMAE	0.91												

In ppm based on the TMS reference, computed at the B3LYP/6-311++G(2df,2pd) level with IEFPCM model in chloroform.

In chloroform using the IEFPCM model ($\epsilon = 4.9$) at B3LYP/6-311++G(2df,2pd) level.MAE: mean absolute error is calculated as $\text{MAE} = \frac{1}{N} \sum_i |\delta_{\text{calc}} - \delta_{\text{exp}}|$.CMAE: corrected mean absolute error is calculated as $\text{CMAE} = \frac{1}{N} \sum_i |\delta_{\text{scale}} - \delta_{\text{exp}}|$.**Fig. 4.** The linear regression between the experimental and theoretical ^{13}C NMR Chemical shifts of MEQ and 1,4-BDM.

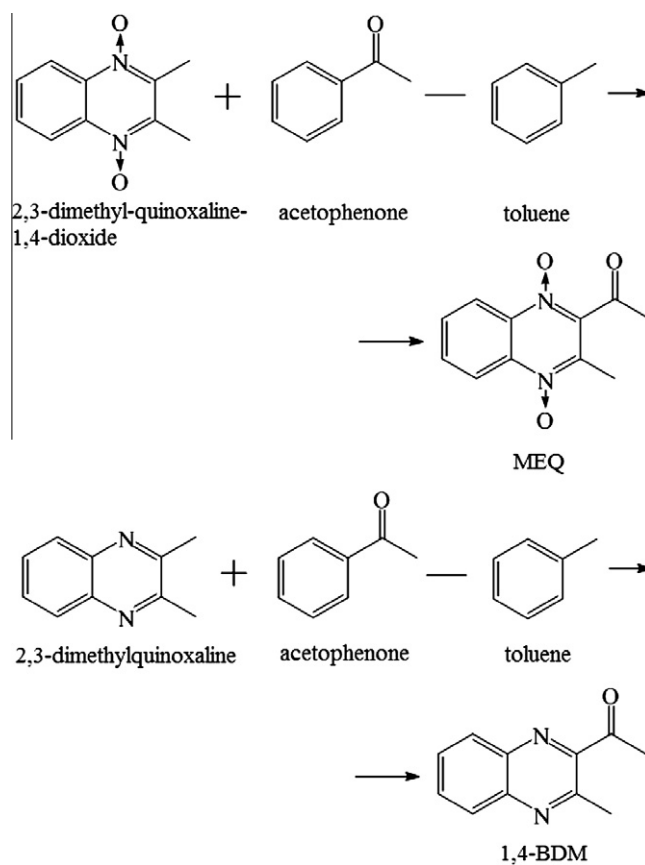
belonging to the quinoxaline moiety fall within 120–132 ppm. The observed chemical shift of protons of the quinoxaline moiety was evidently larger, and protons in 2-methyl showed the lowest values in the results for MEQ and 1,4-BDM.

3.4. Thermochemical studies

As mentioned, the importance of the N–O bonds for selective activity raises an increasing interest in the thermochemical study of the energetic properties of quinoxaline species. The present work reports theoretical results of the DFT calculations of the heat of formation (HOF) for MEQ and 1,4-BDM, and BDE of the N–O bonds. The EOF of MEQ and 1,4-BDM were estimated from the isodesmic reaction approach and a working reaction involving structurally similar reactants and products for which accurate experimental EOF values are known.

The equation shown in Fig. 5 was used in the isodesmic reaction approach, and the literature values of the EOF [$\Delta_f H^\circ(g)$] were the following: 2,3-dimethyl-quinoxaline-1,4-dioxide, $\Delta_f H^\circ(g) = 149.4 \pm 4.5 \text{ kJ mol}^{-1}$ [31]; 2,3-dimethylquinoxaline, $\Delta_f H^\circ(g) = 172.9 \pm 3.0 \text{ kJ mol}^{-1}$ [31]; toluene, $\Delta_f H^\circ(g) = 50.1 \pm 1.1 \text{ kJ mol}^{-1}$ [32]; and acetophenone, $\Delta_f H^\circ(g) = -86.7 \pm 1.7 \text{ kJ mol}^{-1}$ [33]. Similar approaches for estimating the EOF of heteroaromatic nitrogen derivatives (including substituted quinolines) based on well-established experimental values for anchor compounds, have been reported [34].

Using a combination of experimental and B3LYP 6-311++G(2df,2pd) values of anchor compounds based on the isodesmic reaction approach, the theoretical EOF values of MEQ and 1,4-BDM were found to be 44.9 and 51.1 kJ mol^{-1} , respectively.

**Fig. 5.** Working reactions to calculate HOF of MEQ and 1,4-BDM in the isodesmic reaction approach.

The N–O BDE is defined as the enthalpy change of the dissociation reaction in the gas phase at 298.15 K and 1 atm. MEQ has two different N–O bonds, one closer to the methyl group, and the other closer to the acetyl group. Due to the different chemical neighborhoods, these bonds are expected to have different strengths and dissociation energies. Consequently, the N–O BDE may be described in terms of the first, second, total, and mean N–O BDE values. The first N–O BDE is the energy required to break the weakest bonds in the di-N-oxide compound to yield the corresponding N-oxide. The second N–O BDE is the energy required to break the

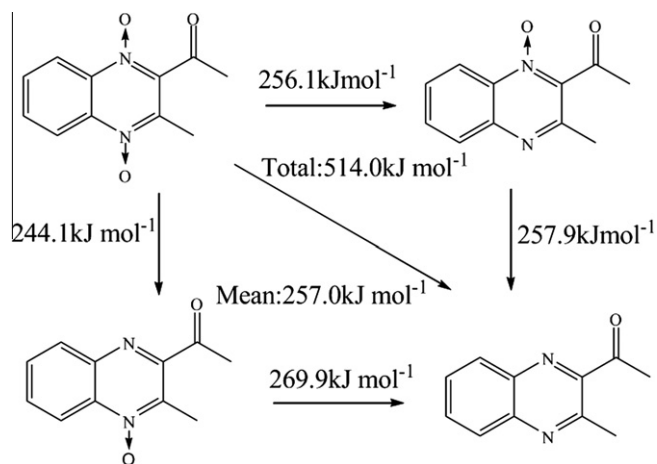


Fig. 6. First, second, total and mean N–O bond dissociation enthalpies for MEQ.

bond in the N-oxide compound to yield the parent quinoxaline. The total N–O BDE and the mean N–O BDE are the sum and mean of the former two dissociation enthalpies, respectively.

The full results for the computed BDEs for MEQ are schematically depicted in Fig. 6. Breaking the 12N–15O bond is easier; the value $244.1 \text{ kJ mol}^{-1}$ was determined to be the first N–O BDE of MEQ (Fig. 6). The corresponding value of the second N–O BDE is $269.9 \text{ kJ mol}^{-1}$, and the total and mean N–O BDEs of MEQ are 514.0 and $257.0 \text{ kJ mol}^{-1}$, respectively.

4. Conclusion

In the present investigation, we have examined the experimental and theoretical molecular conformation and performed the vibrational and NMR analyses of MEQ and 1,4-BDM. The molecular geometry and vibrational frequencies of MEQ and 1,4-BDM have been examined through DFT calculations using the B3LYP functional and 6-311++G(d,p) basis set. In addition, the ^1H and ^{13}C chemical shifts and thermochemical properties have been calculated using the B3LYP 6-311++G(2df,2pd) method.

Optimized geometric structures have been found to be consistent with experimental results. After scaling the values by a factor, the calculated wavenumbers have only minor deviations from the experimental values, and the ^1H and ^{13}C chemical shifts show good agreement with experimental results. The standard molar EOF values of MEQ and 1,4-BDM have also been computed. Finally, the theoretical values of the first, second, total, and mean N–OBDEs for MEQ have been determined using the DFT method. Predicted values based on B3LYP 6-311++G(2df,2pd) are 244.1, 269.9, 514.0, and $257.0 \text{ kJ mol}^{-1}$, respectively.

Acknowledgements

We are grateful to the 973 Fund, the Ministry of Science and Technology, PR China (Grant No. 2009CB118801), Project 20977112

supported by NSFC and Chinese Universities Scientific Fund (Project No. 2011JS035) and the financial support (KY2010G20) from Hubei Key Laboratory of Pollutant Analysis & Reuse Technology.

References

- [1] A. Carta, P. Corona, M. Loriga, *Curr. Med. Chem.* 12 (2005) 2259.
- [2] FAO/WHO. Joint Expert Committee on Food Additives: Evaluation of Certain Veterinary Drug Residues in food. Tech. Ser. 1990, No. 799, 45.
- [3] Z. Liu, L. Huang, M. Dai, D. Chen, Y. Wang, Y. Tao, Z. Yuan, *Rapid Commun. Mass Spectrom.* 22 (2008) 1009.
- [4] X. Huang, A. Ihsan, X. Wang, M. Dai, Y. Wang, S. Su, X. Xue, Z. Yuan, *Toxicol. Lett.* 191 (2009) 167.
- [5] J. Shen, C. Yang, C. Wu, P. Feng, Z. Wang, Y. Li, Y. Li, S. Zhang, *Rapid Commun. Mass Spectrom.* 24 (2010) 375.
- [6] J. Zhang, Q. Peng, S. Zhang, Y. Li, S. Li, H. Gao, Z. Zhou, *J. Mol. Struct.* 987 (2011) 34.
- [7] R. Jain, T. Bally, P.R. Rablen, *J. Org. Chem.* 74 (2009) 4017.
- [8] D.B. Chesnut, *Chem. Phys.* 214 (1997) 73.
- [9] S.P.A. Sauer, V. Spirko, I. Paidarova, W.P. Kraemer, *Chem. Phys.* 214 (1997).
- [10] R.R. Rablen, S.A. Pearlman, J. Finkbinder, *J. Phys. Chem. A* 103 (1999) 214.
- [11] S. Yurdakul, T. Polat, *J. Mol. Struct.* 963 (2010) 194.
- [12] F.D.S. Miranda, A.M. Signori, J. Vicente, B.D. Souza, J.P. Priebe, B. Szpoganicz, N.S. Gonçalves, A. Neves, *Tetrahedron* 64 (2008) 5410.
- [13] H. Zhang, C. Huang, *Environ. Sci. Technol.* 39 (2005) 593.
- [14] X. Zhu, W. Hao, H. Tang, C. Wang, J. Cheng, *J. Am. Chem. Soc.* 127 (2005) 2696.
- [15] R.F. Anderson, S.S. Shinde, M.P. Hay, S.A. Gamage, W.A. Denny, *Org. Biomol. Chem.* 3 (2005) 2167.
- [16] C. Alexandru, M. Fluerau, L.L. Chepelev, J.S. Wright, W.G. Willmore, T. Durst, H.H. Hussain, M. Charron, *Free Radic. Biol. Med.* 38 (2005) 344.
- [17] H. Shadnia, J.S. Wright, *Chem. Res. Toxicol.* 21 (2008) 1197.
- [18] J.M. Brown, W.R. Wilson, *Nat. Rev. Cancer* 4 (2004) 437.
- [19] A.D. Becke, *J. Chem. Phys.* 104 (1996) 1040.
- [20] C. Lee, W. Yang, R.G. Parr, *Phys. Rev. B* 37 (1988) 785.
- [21] M.J. Frisch, G.W. Trucks, H.B. Schlegel, G.E. Scuseria, M.A. Robb, J.R. Cheeseman, G. Scalmani, V. Barone, B. Mennucci, G.A. Petersson, H. Nakatsuji, M. Caricato, X. Li, H.P. Hratchian, A.F. Izmaylov, J. Bloino, G. Zheng, J.L. Sonnenberg, M. Hada, M. Ehara, K. Toyota, R. Fukuda, J. Hasegawa, M. Ishida, T. Nakajima, Y. Honda, O. Kitao, H. Nakai, T. Vreven, J.A. Montgomery, J.E. Peralta, F. Ogliaro, M. Bearpark, J.J. Heyd, E. Brothers, K.N. Kudin, V.N. Staroverov, R. Kobayashi, J. Normand, K. Raghavachari, A. Rendell, J.C. Burant, S.S. Iyengar, J. Tomasi, Gaussian 09, Revision A.02, Gaussian, Inc., Wallingford, CT, 2009.
- [22] J.M.L. Martin, C. Van Alsenoy, GAR2PED Program, University of Antwerpen, Belgium, 1995.
- [23] P. Flukiger, H.P. Luthi, S. Portmann, J. Weber, MOLEKEL, 4.3, Swiss Center for Scientific Computing, Manno, Switzerland, 2000.
- [24] S. Portmann, H.P. Luthi, *Chimia* 54 (2000) 766.
- [25] Y.B. Li, W.F. Zhou, J.L. Wang, H.X. Gao, Z.Q. Zhou, *Acta Cryst. E* 66 (2010) o1801.
- [26] M.A.V. Ribeiro da Silva, M.A.R. Matos, C.M.A. Rio, M.S. Miranda, *J. Phys. Chem. A* 104 (2000) 6644.
- [27] A.P. Scott, L. Radom, *J. Phys. Chem.* 100 (1996) 16502.
- [28] M. Silverstein, G.C. Basseler, C. Morill, *Spectrometric Identification of Organic Compounds*, Wiley, New York, 1981.
- [29] R.J. Kessler, G.N.R. Tripatti, *J. Chem. Phys.* 86 (8) (1987) 4347.
- [30] G. Barone, L. Gomez-Paloma, D. Duca, A. Silvestri, R. Riccio, G. Bifulco, *Chem.-Eur. J.* 8 (2002) 3233.
- [31] Maria D.M.C. Ribeiro da Silva, José R.B. Gomes, Jorge M. Gonçalves, Emanuel A. Sousa, Siddharth Pandey, William E. Acree Jr., *Org. Biomol. Chem.* 2 (2004) 2507.
- [32] M.V. Roux, M. Temprado, J.S. Chickos, Y. Nagano, *J. Phys. Chem. Ref. Data* 37 (2008) 1855.
- [33] J.D. Cox, G. Pilcher, *Thermochemistry of Organic and Organometallic Compounds*, Academic Press, New York, 1970. pp. 1–636.
- [34] M.A.V. Ribeiro da Silva, M.A.R. Matos, *Pure Appl. Chem.* 69 (1997) 2295.